Journal of Alloys and Compounds 513 (2012) 430–435

Contents lists available at SciVerse ScienceDirect

Journal of Alloys and Compounds

journal homepage: www.elsevier.com/locate/jallcom

Luminescence investigation and thermal stability study of Eu^{2+} and Eu^{2+}–Mn^{2+} codoped (Ba,Sr)$Mg_2Al_6Si_9O_{30}$ phosphor

Wei Lü[a,b], Xia Zhang[a,*], Ying Wang[a,b], Zhendong Hao[a], Yongfu Liu[a,b], Yongshi Luo[a], Xiaojun Wang[c], Jiahua Zhang[a,**]

[a] Key Laboratory of Excited State Processes, Changchun Institute of Optics, Fine Mechanics and Physics, Chinese Academy of Sciences, Changchun 130033, China
[b] Graduate School of Chinese Academy of Sciences, Beijing 100039, China
[c] Department of Physics, Georgia Southern University, Statesboro, GA 30460, USA

ARTICLE INFO

Article history:
Received 7 August 2011
Received in revised form 19 October 2011
Accepted 21 October 2011
Available online 7 November 2011

Keywords:
Solid state reactions
Phosphors
Luminescence
Energy transfer

ABSTRACT

Eu^{2+} and Eu^{2+}–Mn^{2+} codoped (Ba,Sr)$Mg_2Al_6Si_9O_{30}$ phosphors have been synthesized by solid state reaction, and their luminescent properties are investigated. Under the excitation of 330 nm, it is observed that the emission of Eu^{2+} consists of two emission bands, located at around 370 and 450 nm, which are attributed to two Eu^{2+} centers (Eu^{2+}(I) and Eu^{2+}(II)) ions substituting for two different Ba^{2+} and Mg^{2+} sites, respectively. As Sr^{2+} gradually substitutes Ba^{2+}, the emission bands of Eu^{2+}(I) shift to longer wavelength whereas the emission bands of Eu^{2+}(II) exhibit no change. This phenomenon is discussed in terms of the crystal-field strength. A detail analysis on the energy transfer from Eu^{2+} to Mn^{2+} in $SrMg_2Al_6Si_9O_{30}$ host is presented, which indicates the energy of the red emission of Mn^{2+} is derived mainly from Eu^{2+}(I). We have also demonstrated that $BaMg_2Al_6Si_9O_{30}$:Eu^{2+}, Mn^{2+} exhibits better thermal quenching properties than that of $SrMg_2Al_6Si_9O_{30}$:Eu^{2+}, Mn^{2+} because of bigger activation energy.

1. Introduction

The quest for new light-emitting-diode (LED) converted phosphors has triggered active research efforts in the investigation of phosphors suitable for UV light excitation. For example, Eu^{2+} and Eu^{3+} as efficient sensitizers have been widely studied for LED in different hosts [1–6]. While, in order to obtain higher color-rendering index and tunable correlated color temperature, doubly doped luminescent material based energy transfer is considered to be an effective alternative for white LEDs. As we known, Mn^{2+} doped luminescent materials have wide-range emissions from 500 to 700 nm depending on the crystal field of the host materials [7–9]. They could be good candidates for red phosphors, but the disadvantage of the Mn^{2+} ions is that their d–d absorption transition is difficult to pump since it is strongly forbidden. Thus, it is necessary to enhance the emission intensity of Mn^{2+} doped materials by introducing Eu^{2+}, would possibly overcome the drawbacks mentioned above. Recently, many phosphors with energy transfer mechanism of Eu^{2+}/Mn^{2+} have been synthesized and investigated in many hosts, such as $Ca_9M(PO_4)_7$ (M = La, Y, Gd, Lu) and $Ca_{10}K(PO_4)_7$ [10–15], they utilized the $Eu^{2+} \rightarrow Mn^{2+}$ energy transfer (ET) to improve the emission intensity of Mn^{2+}. Yang et al. have observed the energy transfer from Eu^{2+} to Mn^{2+} in $BaMg_2(PO_4)_2$, where the Mn^{2+} shows red emission when substituting for Mg^{2+} site [16].

In this work, Eu^{2+} and Eu^{2+}–Mn^{2+} codoped in (Ba,Sr)$Mg_2Al_6Si_9O_{30}$ phosphors are synthesized and their luminescent properties are investigated. The different emission bands of these phosphors are presented, and their origins are to be revealed through the crystal field strength. Energy transfer from Eu^{2+} to Mn^{2+} in $SrMg_2Al_6Si_9O_{30}$ occurs and is systematically investigated by the photoluminescence excitation and emission spectra, and lifetimes. Thermal quenching properties of $BaMg_2Al_6Si_9O_{30}$:Eu^{2+}, Mn^{2+} and $SrMg_2Al_6Si_9O_{30}$:Eu^{2+}, Mn^{2+} are studied.

2. Experimental

2.1. Synthesis

The $(Ba_{0.96-x}Sr_x)Mg_{2-y}Al_6Si_9O_{30}$ ((B,S)MAS):0.04Eu^{2+}, yMn^{2+} phosphors were synthesized by a high-temperature solid-state reaction [17,18]. The constituent oxides or carbonates $BaCO_3$ (99.9%), $SrCO_3$ (99.9%), Al_2O_3 (99.9%), SiO_2 (99.9%), MgO (99.9%), Eu_2O_3 (99.99%), and $MnCO_3$ (99.99%) were employed as the raw materials, which were mixed homogeneously by an agate mortar and pestled for 30 min, placed in a crucible with a lid, and then sintered in a tubular furnace at 1300 °C for 4 h in reductive atmosphere (10% H_2 + 90% N_2 mixed flowing gas). When $x = 0$ and 0.96, the obtained $Ba_{0.96}Mg_{2-y}Al_6Si_9O_{30}$:0.04$Eu^{2+}$, y$Mn^{2+}$ and $Sr_{0.96}Mg_{2-y}Al_6Si_9O_{30}$:0.04$Eu^{2+}$, y$Mn^{2+}$ phosphors were abbreviated as BMAS:0.04Eu^{2+}, yMn^{2+} and SMAS:0.04Eu^{2+}, yMn^{2+}, respectively.

* Corresponding author.
** Corresponding author. Tel: +86 43186176317; fax: +86 43186176317.
E-mail address: zhangjh@ciomp.ac.cn (J. Zhang).

0925-8388/$ – see front matter © 2011 Elsevier B.V. All rights reserved.
doi:10.1016/j.jallcom.2011.10.065

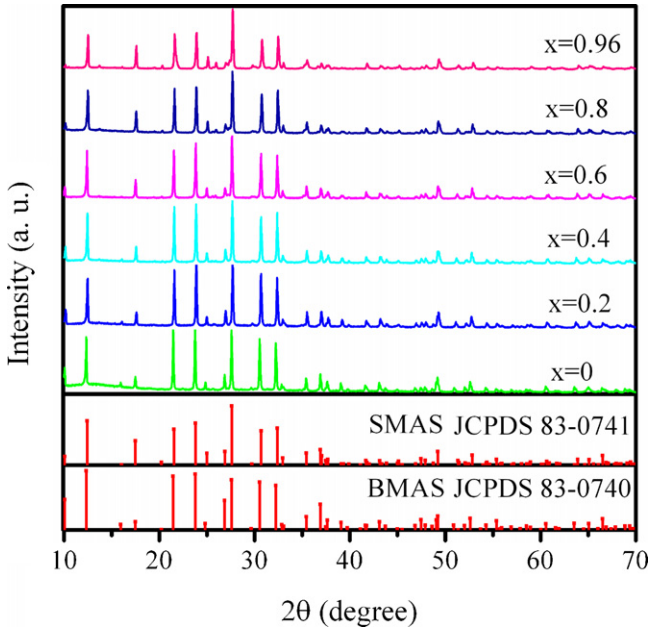

Fig. 1. The representative XRD patterns of the (B,S)MAS:0.04Eu^{2+} samples.

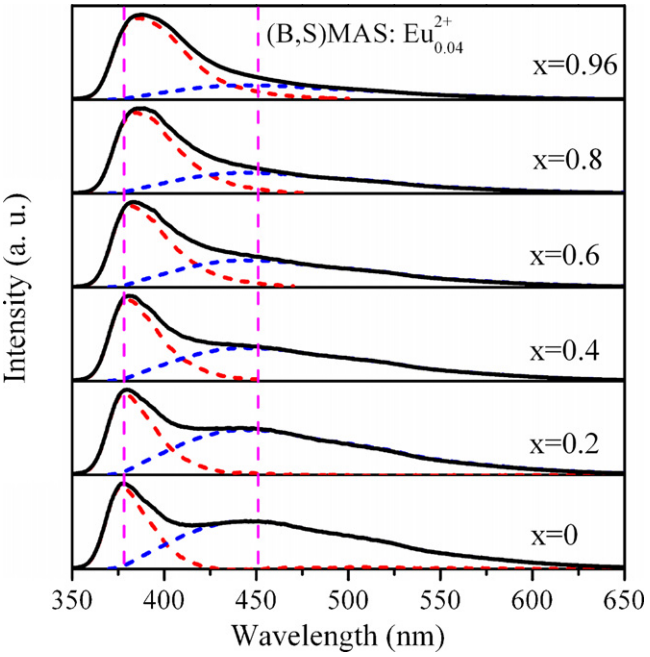

Fig. 2. The PL spectra of the (B,S)MAS:0.04Eu^{2+} phosphors with varying Sr^{2+} ions concentrations (x) at the excitation wavelength of 330 nm.

2.2. Characterization

The structure of sintered samples was identified by an X-ray powder diffractometer (Rigaku D/MAX-2500 V), using Cu Kα radiation (λ = 1.54056 Å). A step size of 0.02° (2θ) was used with a scanning speed of 4°/min. The measurements of photoluminescence (PL) and photoluminescence excitation (PLE) spectra were performed by using a Hitachi F4500 spectrometer equipped with a 150 W xenon lamp under a working voltage of 700 V. The excitation and emission slits were both set at 2.5 nm. In fluorescence lifetime measurements, the third harmonic (355 nm) of an Nd-doped yttrium aluminum garnet pulsed laser (Spectra-Physics, GCR 130) was used as an excitation source, and the signals were detected with a Tektronix digital oscilloscope (TDS 3052).

3. Results and discussion

3.1. Phase analysis

Fig. 1 presents the representative XRD patterns of the (B,S)MAS:0.04Eu^{2+} samples. All of the diffraction peaks are indexed to the standard data of $BaMg_2Al_6Si_9O_{30}$ and $Sr_{0.91}Mg_2Al_{5.82}Si_{9.18}O_{30}$ (JPCDS card no. 83-0740 and 83-0741) [19] and no diffraction peaks from the raw materials are detected, indicating that the increasing x do not significantly influence the structure. (B,S)MAS crystallize in hexagonal structure with space group $P6/mcc$ and have two type independent cation sites, 12-fold coordinated M^{2+} (M = Ba or Sr) site and 6-fold coordinated Mg^{2+} site. In our previous work, it is demonstrated that the PL spectrum of Eu^{2+} in BMAS exhibits two PL bands, which indicates Eu^{2+} ions in different sites [20]. Therefore it is speculated that Eu^{2+} ions can only substitute Ba^{2+}/Sr^{2+} and Mg^{2+} sites despite the ionic radius of Mg^{2+} is too small for Eu^{2+}. In addition, some published papers also reported that Eu^{2+} can substitute Mg^{2+} sites [21–23], such as in $Ba_2Mg(BO_3)_2$.

3.2. Luminescence properties of (B,S)MAS:Eu^{2+}

The PL spectra of the (B,S)MAS:0.04Eu^{2+} phosphors with varying Sr^{2+} ions concentrations (x) are illustrated in Fig. 2. The PL spectra consist of two bands: Eu^{2+}(I) of a shorter wavelength emission is assigned to Eu^{2+} occupying Ba^{2+} or Sr^{2+} with weak crystal field and Eu^{2+}(II) of a longer wavelength emission corresponds to Eu^{2+} occupying Mg^{2+} with strong crystal field. In the case of BMAS:0.04Eu^{2+}, one band is located around 370 nm with a full width at half maximum (FWHM) of 26 nm, and the other band is positioned at 450 nm with a FWHM of 125 nm, these results are in agreement with our previous work [20]. By changing the x value from 0.2 to 0.96, the emission peaks of Eu^{2+}(I) shift gradually to longer wavelength from 376 to 388 nm and the FWHM increases from 26 nm for BMAS:0.04Eu^{2+} to 41 nm SMAS:0.04Eu^{2+}. This phenomenon can be explained in terms of the crystal field. The crystal field strength is increased with a decrease in bond length by replacing with smaller M cations; $D_q \propto 1/R^5$ where D_q is the crystal field, R is the bond length between a center ion and ligand ions [24]. Therefore, in the present system, the crystal field strength will be larger as Sr^{2+} substitutes Ba^{2+}, which results in the redshift of Eu^{2+}(I) of longer wavelength. While the PL peaks of Eu^{2+}(II) keep unchanged because Eu^{2+}(II) ions always occupy Mg^{2+} with similar crystal field environments. It is also noticed that the relative intensity of Eu^{2+}(II) decreases remarkably. It suggests that Sr content (x) did affect the distribution of Eu^{2+} in different sites. In fact, the ionic radii Eu^{2+}(1.17 Å for CN = 6, 1.26 Å for CN = 12) is much bigger than Mg^{2+} (0.72 Å, CN = 6), but much smaller than Ba^{2+} (1.61 Å, CN = 12) in BMAS. It is therefore understood that a part of Eu^{2+} ions can substitute Mg^{2+} sites, leading to the 450 nm emission. As the increase of Sr amount, Eu^{2+} substitution for Mg^{2+} should be limited because the ionic radii of Sr^{2+} (1.44 Å, CN = 12) are more closer to Eu^{2+}, which finally results in the decrease of Eu^{2+}(II) emission.

Decay curves of BMAS:Eu^{2+} and SMAS:Eu^{2+} phosphors are depicted in Fig. 3. The decay time of Eu^{2+}(I) in SMAS:Eu^{2+} is little shorter than that in BMAS:Eu^{2+}, due to the increase in non-radiative rates caused by the increase in the phonon coupling [24]. As a result, the shorter decay time of SMAS:Eu^{2+} results in the increase in FWHM of the emission spectrum of Eu^{2+}(I) as seen in Fig. 2. This is similar to the results observed in case of $(Ba,Ca)_2SiO_4$:Eu^{2+} [25].

3.3. Luminescence properties and energy transfer in (B,S)MAS:Eu^{2+}, Mn^{2+}

Fig. 4 shows the PL spectra of (B,S)MAS:Eu^{2+}, Mn^{2+} with varying Sr content x (x = 0, 0.2, 0.4, 0.6, 0.8, 0.96) at fixed Eu^{2+} and Mn^{2+}

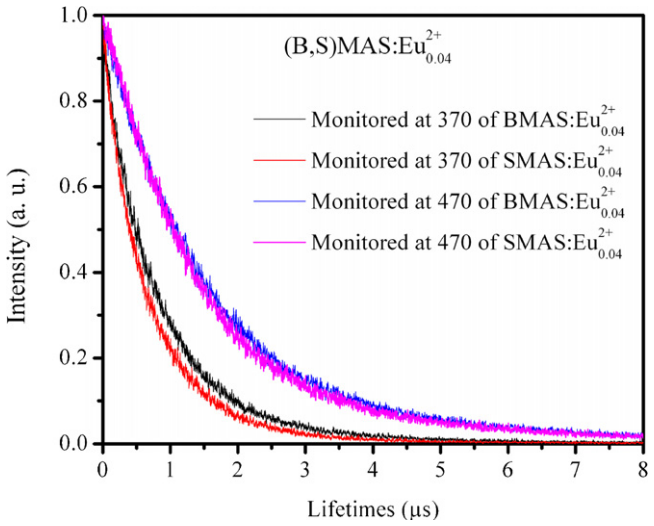

Fig. 3. Decay curves of BMAS:Eu^{2+} and SMAS:Eu^{2+} phosphors.

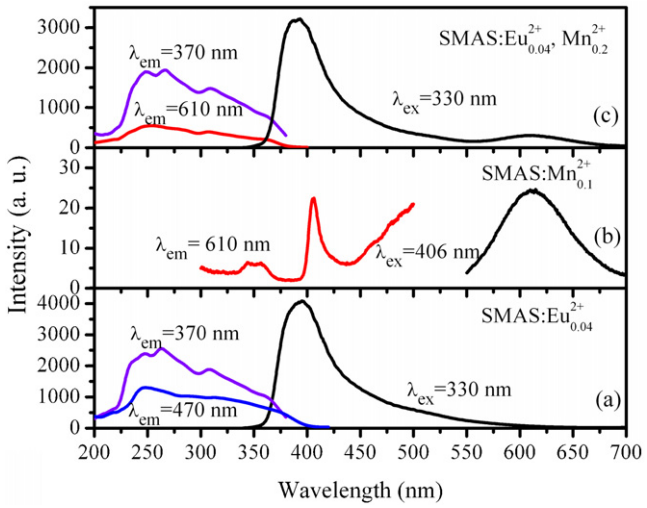

Fig. 5. The excitation and emission spectra of SMAS:Eu^{2+}(a), SMAS:Mn^{2+} (b) and SMAS:Eu^{2+}, Mn^{2+}(c) phosphors.

concentrations. Under the excitation of 330 nm, the emission spectra of (B,S)MAS:Eu^{2+}, Mn^{2+} appear not only as a strong band of the Eu^{2+} ions range from 350 to 600 nm but also as a red band peaking at 610 nm of the Mn^{2+} ions. With increasing x concentration, the emission bands at 610 nm do not change, which result from little changes in the crystal field around Mn^{2+}.

In our pervious work, we have demonstrated that energy transfer from Eu^{2+} to Mn^{2+}in BMAS host matrix. Thus, in this study, we focus on investigating the energy transfer in SMAS host. The PL spectra of Eu^{2+} and the PLE spectra of Mn^{2+} singly doped phosphors are shown in Fig. 5(a) and (b). SMAS:Mn^{2+} exhibits a very weak red emission band peaking at 610 nm originating from $^4T_1$–$^6A_1$ transition of Mn^{2+} with its PLE peaks at 355 and 406 nm, corresponding to the forbidden transitions from the ground state $^6A_1(6_S)$ to $^4T_2(^4D)$ and ($^4A_1(^4G)$, $^4E(^4G)$) levels of Mn^{2+}, respectively [26]. Fig. 5(c) shows the PLE and PL spectra of SMAS:0.04Eu^{2+}, 0.2Mn^{2+}, the PLE spectrum monitoring the red emission of the Mn^{2+} is more similar to that monitoring the Eu(I) emission, indicating the energy transfer occurred mainly from Eu^{2+}(I) to Mn^{2+}. In order to further investigate the energy transfer process between the Eu^{2+} and Mn^{2+} ions in SMAS, a series of samples are prepared. Fig. 6 shows the PL spectra of SMAS:0.01Eu^{2+}, $y$$Mn^{2+}$ phosphors with different doping contents y, which were measured at the excitation wavelength of 330 nm. With the doping Mn^{2+} concentration increasing, the emission intensity of the Mn^{2+} ions increases systematically and reaches saturation when y is equal to about 0.24. These results indicate that the energy transfer from the Eu^{2+} to Mn^{2+} ions.

The fluorescence lifetimes of 370 (τ_1), 470 (τ_2) emissions in SMAS:0.01Eu^{2+}, $y$$Mn^{2+}$($y$ = 0, 0.04, 0.08, 0.12, 0.16, 0.2 and 0.24) are measured and presented in Fig. 7(a) and (b). The reduction of the lifetimes for Eu^{2+} at different luminescence center with increasing Mn^{2+} concentrations are observed, which is a strong evidence for the energy transfer from the Eu^{2+} to Mn^{2+} ions.

The energy transfer processes can be described as follows: the three emitting centers at 370, 470, and 610 nm are labeled by 1, 2, and 3, respectively, and the energy transfer from their center is considered. The energy transfer efficiency can be obtained using $\eta_{Eu-Mn} = 1 - \tau/\tau_0$, as shown in Fig. 7(a) and (b) inset. It can be seen that the values of η_{13} and η_{23} gradually increase and reach to 30% of Eu^{2+}(I) and 21% of Eu^{2+}(II) for Mn^{2+} concentrations at y = 0.24. In continuous excitation, the number of Eu^{2+} excited state rate equation for center 1, 2 with 3 has the relationship as:

$$W_{13}n_1 + W_{23}n_2 = \frac{n_3}{\tau_3} \quad (1)$$

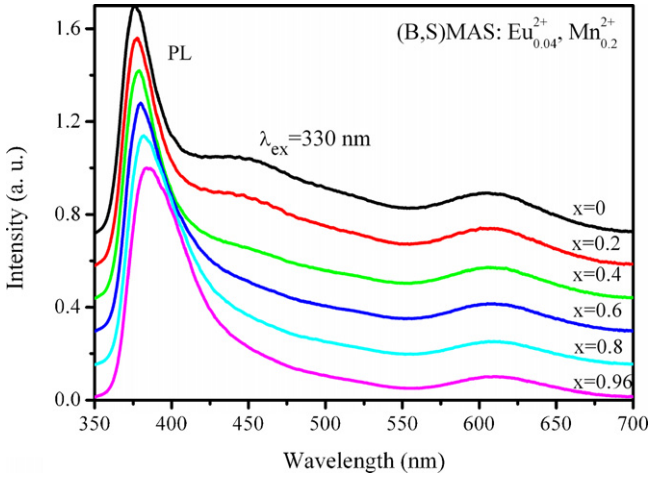

Fig. 4. The PL spectra of (B,S)MAS:0.04Eu^{2+}, 0.2Mn^{2+} with varying Sr content x (x = 0, 0.2, 0.4, 0.6, 0.8, 0.96) at fixed Eu^{2+} and Mn^{2+} concentrations.

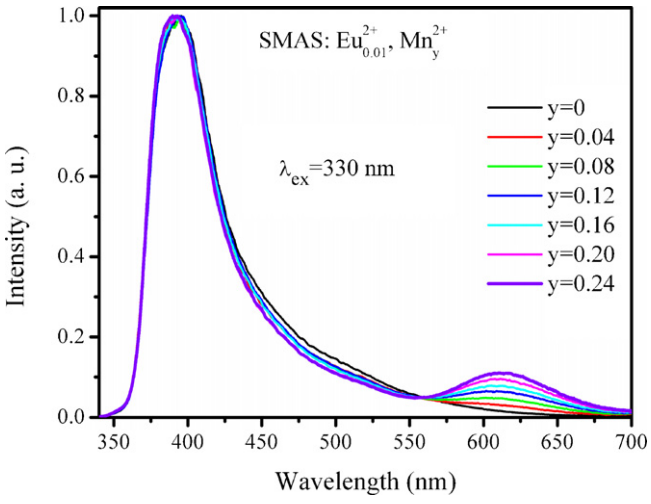

Fig. 6. The PL spectra of SMAS:0.01Eu^{2+}, $y$$Mn^{2+}$ phosphors with different doping contents y at the excitation wavelength of 330 nm.

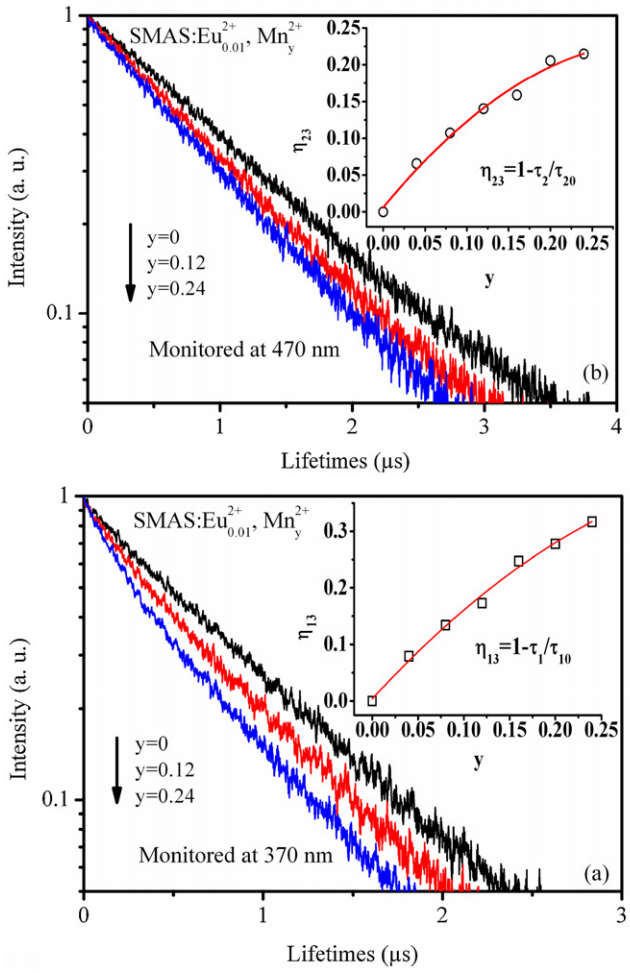

Fig. 7. The fluorescence lifetimes of Eu^{2+}(I) (τ_1) (a) and Eu^{2+}(II) (τ_2) (b) in SMAS:0.01Eu^{2+}, yMn^{2+} (y = 0, 0.04, 0.08, 0.12, 0.16, 0.2 and 0.24). Inset: the energy transfer efficiency (η_{Eu-Mn}) with different doping Mn^{2+} contents.

where n_i and W_{i3} are population of center i and energy transfer rate from center i to center 3, respectively. τ_3 is the fluorescence lifetime of Mn^{2+}. If the emission intensity and radiative transition rate of center i are denoted by I_i and γ_i, the intensity ratio of the red emission of Mn^{2+} to the emission of Eu^{2+} is determined by the following equation:

$$\frac{I_3}{I_1+I_2} = \tau_3\gamma_3\left(\frac{W_{13}I_1}{\gamma_1(I_1+I_2)} + \frac{W_{23}I_2}{\gamma_2(I_1+I_2)}\right) \quad (2)$$

where $W_{13} = 1/\tau_1 - 1/\tau_{10}$, $W_{23} = 1/\tau_2 - 1/\tau_{20}$; τ_{10} and τ_{20} is the fluorescence lifetime of Eu^{2+}(I) and Eu^{2+}(II) in absence of Mn^{2+}, respectively. The $I_3/(I_2+I_1)$ integral intensity ratio of the Mn^{2+} emission to the Eu^{2+} emission can be calculated according to the emission spectra in Fig. 6. The γ_1 and γ_2 are obtained from intrinsic lifetime measurements of 370 nm and 470 nm emissions, respectively, in SMAS:0.005Eu^{2+} to avoid concentration and nonradiative transition effects. τ_3 has been measured and nearly unchanged for different Mn^{2+} concentrations. The $I_3/(I_2+I_1)$ intensity ratios at various Mn^{2+} concentrations are calculated using Eq. (2) and scaled to the maximum, as presented in Fig. 8. For comparison, the intensity ratios obtained directly from the emission spectra are also given in Fig. 8. It can be seen that the calculated data are in good agreement with the experimental ones. Noteworthy, since the energy of Mn^{2+} can be estimated using Eq. (2) from the contribution of Eu^{2+}(I) and Eu^{2+}(II), it is found that the contribution of Eu^{2+}(I) is 7 times larger

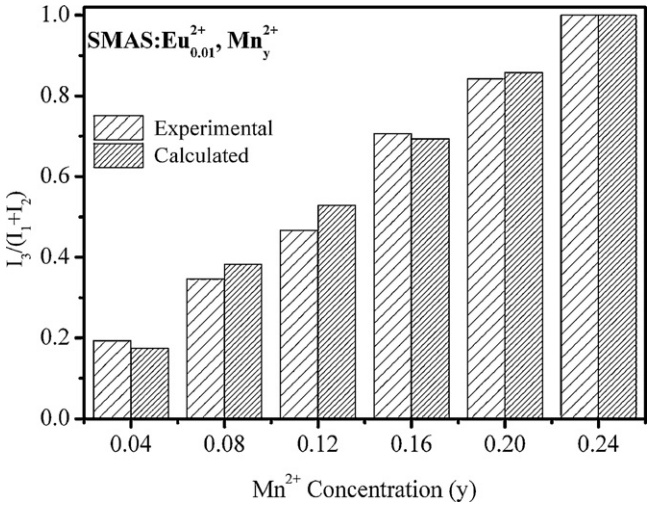

Fig. 8. Calculated and experimental ratios of $I_3/(I_1+I_2)$ intensity ratios at various Mn^{2+} concentrations. The ratios are scaled to the maximum.

than that of Eu^{2+}(II) for SMAS:0.04Eu^{2+}, 0.2Mn^{2+} sample, further implying the energy of Mn^{2+} mainly come from Eu^{2+}(I).

3.4. Thermal stability study of BMAS:Eu^{2+}, Mn^{2+} and SMAS:Eu^{2+}, Mn^{2+} phosphors

In the white LED application, a low-temperature quenching effect is in favor of keeping the chromaticity and brightness of white light output. The temperature-dependent emission intensity of the optimized BMAS:0.04Eu^{2+}, 0.2Mn^{2+} and SMAS:0.04Eu^{2+}, 0.2Mn^{2+} samples are shown in Figs. 9 and 10. As the temperature rises from 30 °C to 150 °C at which the white LEDs usually work, the emission intensity of both the Eu^{2+} and Mn^{2+} emissions remains at about 88% of that measured at room temperature, which are nearly as good as YAG:Ce in terms of their thermal quenching properties [20]. The decrease in emission intensity with increasing temperature originates from a temperature-dependent phonon-coupling factor, which can be explained by thermal quenching at configurational coordinate diagram [24]. The excited luminescent center is thermally activated through phonon interaction, and then thermally released through the crossing point between the excite state and the ground state. It is noticed that the PL intensity of BMAS:Eu^{2+}, Mn^{2+} decreases slower than that in SMAS:Eu^{2+}, Mn^{2+} phosphor as temperature rises. This behavior is understood in terms of two reasons: first, in the configurational coordinate diagram, in the case of BMAS:Eu^{2+}, Mn^{2+} to SMAS:Eu^{2+}, Mn^{2+} activation energy decreases with increasing Stokes shift, leading to decreasing the nonradiative barrier from the excited state to the ground state, consequently the samples are quenched at lower temperature. Second, the vibrational frequency will increase as Ba^{2+} ions are completed substituted by Sr^{2+} ions. The higher vibrational frequency enhances the crossover relaxation from the excited state to the ground state [27]. According to the classical theory of thermal quenching, the temperature dependent PL intensity can be described by the equation

$$I(T) = \frac{I(0)}{1 + A\ \exp(-\Delta E/k_B T)} \quad (3)$$

with constant A, activation energy ΔE and Boltzmann constant k_B [28]. The experimental data are well fitted by Eq. (3), as shown in Fig. 10. An activation energy of Eu^{2+} in BMAS:Eu^{2+}, Mn^{2+} is 0.25 eV, which is bigger than that for SMAS:Eu^{2+}, Mn^{2+} phosphor with ΔE = 0.14 eV. In addition, an activation energy of Mn^{2+} in BMAS:Eu^{2+}, Mn^{2+} and SMAS:Eu^{2+}, Mn^{2+} are both 0.17 eV. This is

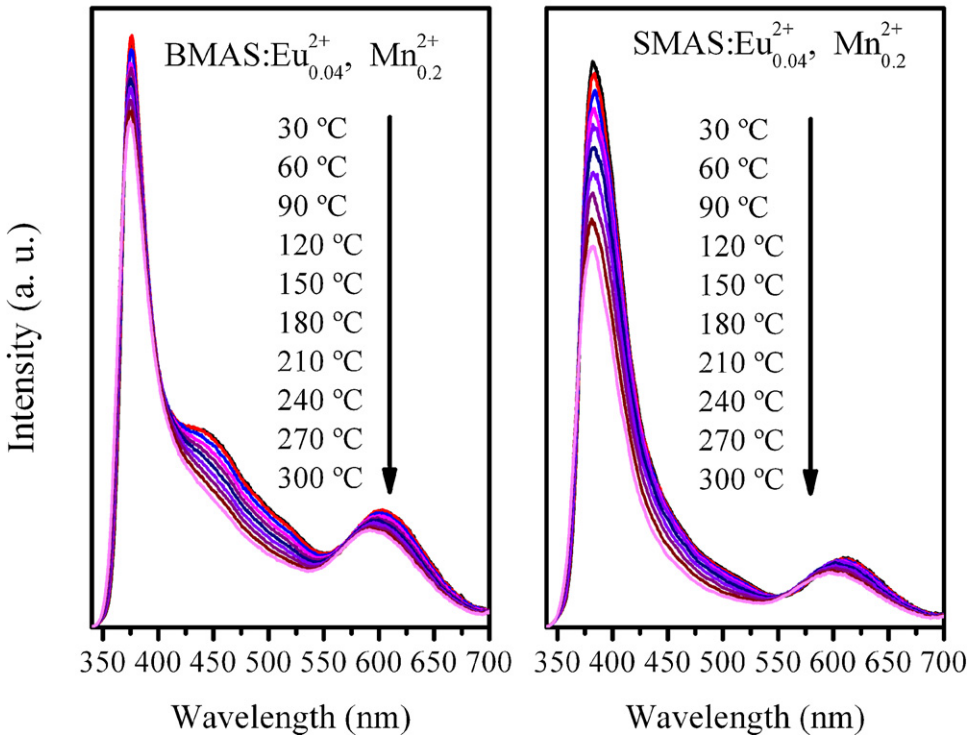

Fig. 9. The temperature-dependent emission intensity of the BMAS:0.04Eu^{2+}, 0.2Mn^{2+} and SMAS:0.04Eu^{2+}, 0.2Mn^{2+} samples.

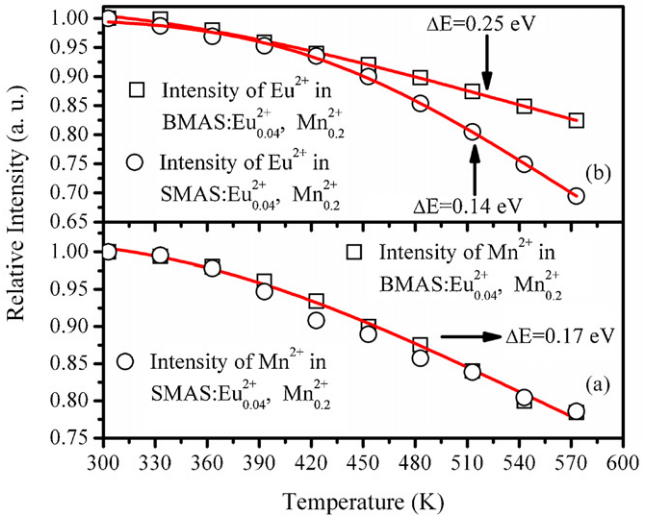

Fig. 10. Temperature dependence of PL intensity of Eu^{2+} and Mn^{2+} in BMAS:0.04Eu^{2+}, 0.2Mn^{2+} and SMAS:0.04Eu^{2+}, 0.2Mn^{2+} under excitation at 330 nm. The dots and squares are experimental data and the lines are fitting functions.

why the BMAS:Eu^{2+}, Mn^{2+} phosphor exhibits a better temperature characteristic.

4. Conclusions

In summary, we have synthesized a series of (Ba,Sr)$Mg_2Al_6Si_9O_{30}$:Eu^{2+} and (Ba,Sr)$Mg_2Al_6Si_9O_{30}$:Eu^{2+}, Mn^{2+} phosphors by solid state reaction. Their luminescent properties are investigated. (Ba,Sr)$Mg_2Al_6Si_9O_{30}$:Eu^{2+} show two emission bands, corresponding to Eu^{2+} ions doped into two different cation sites in host lattices. When the crystal phase of the phosphors gradually changes from BMAS to SMAS, the shorter wavelength emission bands are redshifted due to the increase in crystal field of Eu^{2+}(I), while the longer wavelength emission bands do not change because of little change of Eu^{2+}(II) in crystal field. The energy transfer from Eu^{2+} to Mn^{2+} in (Ba,Sr)$Mg_2Al_6Si_9O_{30}$ host matrix is demonstrated leads to the following results: (1) the energy of the red emission of Mn^{2+} is considered to come mainly from Eu^{2+}(I) and (2) the ratio of the red emission of Mn^{2+} to the emission of Eu^{2+} by experiment is consistent with the theoretical calculation basing on energy transfer and lifetime measurements. We have also demonstrated that $BaMg_2Al_6Si_9O_{30}$:Eu^{2+}, Mn^{2+} exhibited better thermal quenching properties than that of $SrMg_2Al_6Si_9O_{30}$:Eu^{2+}, Mn^{2+} because of bigger activation energy.

Acknowledgements

This work is financially supported by the National Nature Science Foundation of China (10834006, 10904141, 10904140, 51172226), the MOST of china (2010AA03A404) and the Scientific project of Jilin province (20090134, 20090524) and CAS Innovation Program.

References

[1] C.F. Guo, Y. Xu, X. Ding, M. Li, J. Yu, Z.Y. Ren, J.T. Bai, J. Alloys Compd. 509 (2011) L38–L41.
[2] K. Shioi, Y. Michiue, N. Hirosaki, R.J. Xie, T. Takeda, Y. Matsushita, M. Tanaka, Y.Q. Li, J. Alloys Compd. 509 (2011) 332–337.
[3] Q.X. Li, J.P. Huang, D.H. Chen, J. Alloys Compd. 509 (2011) 1007–1010.
[4] S.A. Yana, Y.S. Chang, W.S. Hwang, Y.H. Chang, M. Yoshimura, C.S. Hwang, J. Alloys Compd. 509 (2011) 5777–5782.
[5] Z.D. Hao, J.H. Zhang, X. Zhang, X.J. Wang, Opt. Mater. 33 (2011) 355–358.
[6] Y. Gandhi, I.V. Kityk, M.G. Brik, P.R. Rao, N. Veeraiah, J. Alloys Compd. 508 (2010) 278–291.
[7] J.S. Kim, P.E. Jeon, Y.H. Park, J.C. Choi, H.L. Park, G.C. Kim, T.W. Kim, Appl. Phys. Lett. 85 (17) (2004) 3696–3698.
[8] Z.D. Hao, J.H. Zhang, X. Zhang, X.Y. Sun, Y.S. Luo, S.Z. Lu, X.J. Wang, Appl. Phys. Lett. 90 (26) (2007) 261113–261123.
[9] G. Zhu, Y.H. Wang, Z.P. Ci, B.T. Liu, Y.R. Shi, S.Y. Xin, J. Electrochem. Soc. 158 (8) (2011) J236–J242.

[10] C.H. Huang, T.M. Chen, Opt. Express 18 (2010) 5089–5099.
[11] C.H. Huang, T.M. Chen, W.R. Liu, Y.C. Chiu, Y.T. Yeh, S.M. Jang, ACS Appl. Mater. Int. 2 (2010) 259–264.
[12] C.H. Huang, W.R. Liu, T.M. Chen, J. Phys. Chem. C 114 (2010) 18698–18701.
[13] N. Guo, H.P. You, Y.H. Song, M. Yang, K. Liu, Y.H. Zheng, Y.J. Huang, H.J. Zhang, J. Mater. Chem. 20 (2010) 9061–9067.
[14] N. Guo, Y.J. Huang, H.P. You, M. Yang, Y.H. Song, K. Liu, Y.H. Zheng, Inorg. Chem. 49 (23) (2010) 10907–10913.
[15] W.R. Liu, Y.C. Chiu, Y.T. Yeh, S.M. Jang, T.M. Chen, J. Electrochem. Soc. 156 (7) (2009) J165–J169.
[16] Z.P. Yang, S.Y. Ma, H.W. Yu, F.G. Wang, X. Ma, Y.F. Liu, P.L. Li, J. Alloys Compd. 509 (2011) 76–79.
[17] USPTO Patent Application 20100259161.
[18] Korean Patent Application No. 10-2009-0030957.
[19] W. Wolfgang, T. Armbruster, C. Lengauer, Eur. J. Miner. 7 (1995) 277–286.
[20] W. Lü, Z.D. Hao, X. Zhang, Y.S. Luo, X.J. Wang, J.H. Zhang, Inorg. Chem. 50 (2011) 7846–7851.
[21] S.L. Yuan, Y.X. Yang, X.H. Zhang, F. Tessier, F. Cheviré, J.L. Adam, B. Moine, G.R. Chen, Opt. Lett. 33 (2008) 2865–2867.
[22] B.Y. Han, S.P. Singh, K.S. Sohn, J. Electrochem. Soc. 158 (2) (2011) J32–J35.
[23] L. Lin, C.S. Shi, Z.F. Wang, W.P. Zhang, M. Yin, J. Alloys Compd. 466 (2008) 546–550.
[24] B. Henderson, G.G. Imbush, Optical Spectroscopy of Inorganic Solids, Clarendon, Oxford, 1989.
[25] J.S. Kim, P.E. Jeon, J.C. Choi, H.L. Park, Solid State Commun. 133 (2005) 187–190.
[26] W.J. Yang, L.Y. Luo, T.M. Chen, N.S. Wang, Chem. Mater. 17 (2005) 3883–3888.
[27] R.C. Ropp, Luminescence and the Solid State, Elsevier, New York, 1991.
[28] Y.H. Chen, B. Liu, C.S. Shi, G.H. Ren, G. Zimmerer, Nucl. Instrum. Methods Phys. Res. A 537 (2005) 31–35.